Geomechanics and Engineering, *Vol. 16, No. 1 (2018) 1-9*
DOI: https://doi.org/10.12989/gae.2018.16.1.001

An efficient and simple refined theory for free vibration of functionally graded plates under various boundary conditions

Nafissa Zouatnia[1], Lazreg Hadji*[2,3] and Amar Kassoul[1]

[1]*Department of Civil Engineering, Laboratory of Structures, Geotechnics and Risks (LSGR), Hassiba Benbouali University of Chlef, Algeria, BP 151, Hay Essalam, UHB Chlef, Chlef (02000), Algeria*
[2]*Department of Civil Engineering, Ibn Khaldoun University, BP 78 Zaaroura, Tiaret (14000), Algeria*
[3]*Laboratory of Geomatics and Sustainable Development, Ibn Khaldoun University of Tiaret, Algeria*

(Received June 1, 2017, Revised February 28, 2018, Accepted March 6, 2018)

Abstract. In this paper an efficient and simple refined shear deformation theory is presented for the free vibration of Functionally Graded Plates Under Various Boundary Conditions. The theory accounts for a quadratic variation of the transverse shear strains across the thickness, and satisfies the zero traction boundary conditions on the top and bottom surfaces of the plate without using shear correction factors. The number of independent unknowns of present theory is four, as against five in other shear deformation theories. The plates are considered of the type having two opposite sides simply-supported, and the two other sides having combinations of simply-supported, clamped, and free boundary conditions. The mechanical properties of functionally graded material are assumed to vary according to power law distribution of the volume fraction of the constituents. Equations of motion are derived using Hamilton's principle. The results of this theory are compared with those of other shear deformation theories. Various numerical results including the effect of boundary conditions, power-law index, plate aspect ratio, and side-to-thickness ratio on the free vibration of FGM plates are presented.

Keywords: free vibration; functionally graded materials; boundary conditions; shear deformation theories; Hamilton's principle

1. Introduction

Functionally graded materials (FGMs) are a class of composites that have continuous variation of material properties from one surface to another and thus eliminate the stress concentration found in laminated composites. A typical FGM is made from a mixture of two material phases, for example, a ceramic and a metal. The reason for the increasing use of FGMs in a variety of aerospace, automotive, civil, and mechanical engineering structures is that their material properties can be tailored to different applications and working environments. Now, FGMs are developed for general use as structural components in extremely high temperature environments. Several studies have been performed to analyze the mechanical or the thermal or the thermomechanical responses of FG plates and shells.

Tai *et al.* (2011) used levy-type solution for buckling analysis of orthotropic plates based on two variable refined plate theory. Tai *et al.* (2012) developed the Levy-type solution for free vibration analysis of orthotropic plates based on two variable refined plate theory. Sobhy *et al.* (2013) studied the buckling and free vibration of exponentially graded sandwich plates resting on elastic foundations under various boundary conditions. Tahouneh (2014) studied the free vibration analysis of bidirectional functionally graded annular plates resting on elastic foundations using differential quadrature method. Belabed *et al.* (2014) used an efficient and simple higher order shear and normal deformation theory for functionally graded material (FGM) plates. Hamidi *et al.* (2015) proposed a sinusoidal plate theory with 5-unknowns and stretching effect for thermomechanical bending of functionally graded sandwich plates. Hebali *et al.* (2014) used a new quasi-3D hyperbolic shear deformation theory for the static and free vibration analysis of functionally graded plates. Farahani *et al.* (2015) investigated the vibration of sumberged functionally graded cylindrical shell based on first order shear deformation theory using wave propagation method. Deng *et al.* (2015) studied the analysis of thermally induced vibration of cable-beam structures. Gao *et al.* (2015) used the refined theory of 2D quasicrystal deep beams based on elasticity of quasicrystals. Al-Basyouni *et al.* (2015) investigated size dependent bending and vibration analysis of functionally graded micro beams based on modified couple stress theory and neutral surface position. Benferhat *et al.* (2016) studied the effect porosities on Static analysis of the FGM plate. Meziane *et al.* (2014) proposed an efficient and simple refined theory for buckling and free vibration of exponentially graded sandwich plates under various boundary conditions. Recently Tai *et al.* (2014) used levy Solution for free vibration analysis of functionally graded plates based on a refined plate theory. Merazi *et al.* (2015) used a new hyperbolic shear deformation plate theory for static analysis of FGM plate based on neutral

*Corresponding author, Ph.D.
E-mail: had_laz@yahoo.fr

ISSN: 2005-307X (Print), 2092-6219 (Online)

surface position. Benbakhti et al. (2016) used a new five unknown quasi-3D type HSDT for thermomechanical bending analysis of FGM sandwich plates. Ghorbanpour *et al.* (2017) studied the vibration analysis of functionally graded nanocomposite plate moving in two directions. Hadji *et al.* (2017) studied the wave propagation in functionally graded beams using various higher-order shear deformation beams theories. Houari *et al.* (2017) investigated a novel quasi-3D hyperbolic shear deformation theory for Functionally Graded thick rectangular Plates on elastic foundation.

This work aims to develop an efficient and simple refined shear deformation theory for the free vibration analyses of functionally graded plates under various boundary conditions. Equations of motion are derived from the Hamilton's principle. In this study the plates are considered of the type having two opposite sides simply-supported, and the two other sides having combinations of simply-supported, clamped, and free boundary conditions. Comparison studies are performed to verify the validity of the present results. The effects of boundary condition and aspect ratio, and thickness ratio on the natural frequencies of FG plates are studied and discussed in detail.

2. Theoretical formulation

2.1 Plate construction

Consider a FG rectangular plate occupying the region $[0,a]x[0,b]x[-h/2,+h/2]$ from the coordinate system (x; y; z) as shown in Fig. 1. This plate is made of an isotropic material with material properties varying smoothly in the z (thickness) direction only. We assume that the composition is varied from the bottom to the top surfaces, i.e. the bottom surface $(z=-h/2)$ of the plate is metal rich whereas the top surface $(z=+h/2)$ is ceramic-rich.

The mechanical properties of FGM such as Young's modulus E and mass density ρ can be expressed as

$$E(z)=E_m+(E_c-E_m)\left(\frac{z}{h}+\frac{1}{2}\right)^k$$
$$\rho(z)=\rho_m+(\rho_c-\rho_m)\left(\frac{z}{h}+\frac{1}{2}\right)^k \quad (1)$$

where the subscripts m and c represent the metallic and ceramic constituents, respectively; and p is the volume fraction exponent. The value of k equal to zero represents a fully ceramic plate, whereas infinite p indicates a fully metallic plate. The variation of Poisson's ratio v is generally small and it is assumed to be a constant for convenience. The linear constitutive relations of a FG plate can be written as

$$\begin{Bmatrix}\sigma_x\\ \sigma_y\\ \tau_{xy}\end{Bmatrix}=\begin{bmatrix}Q_{11} & Q_{12} & 0\\ Q_{12} & Q_{22} & 0\\ 0 & 0 & Q_{66}\end{bmatrix}\begin{Bmatrix}\varepsilon_x\\ \varepsilon_y\\ \gamma_{xy}\end{Bmatrix} \quad (2)$$

$$\text{and}\quad \begin{Bmatrix}\tau_{yz}\\ \tau_{zx}\end{Bmatrix}=\begin{bmatrix}Q_{44} & 0\\ 0 & Q_{55}\end{bmatrix}\begin{Bmatrix}\gamma_{yz}\\ \gamma_{zx}\end{Bmatrix}$$

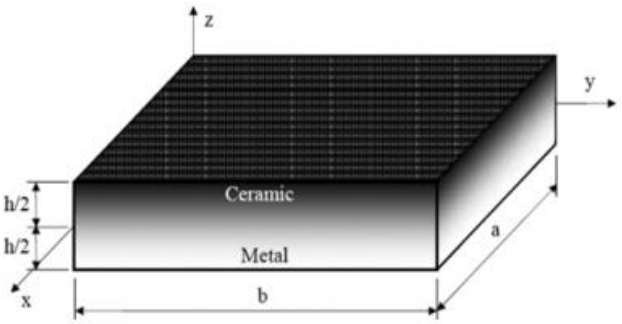

Fig. 1 Geometry of rectangular FG plate and coordinates

where

$$Q_{11}=Q_{22}=\frac{E(z)}{1-\nu^2}$$
$$Q_{12}=\frac{\nu\,E(z)}{1-\nu^2} \quad (3)$$
$$Q_{44}=Q_{55}=Q_{66}=\frac{E(z)}{2(1+\nu)}$$

2.2 Displacement field

The displacement field, taking into account the shear deformation effect, is presented for FGM structures as

$$U(x,y,z,t)=u_0(x,y,t)-z\frac{\partial w_b}{\partial x}-f(z)\frac{\partial w_s}{\partial x}$$
$$V(x,y,z,t)=v_0(x,y,t)-z\frac{\partial w_b}{\partial y}-f(z)\frac{\partial w_s}{\partial y} \quad (4)$$
$$W(x,y,z,t)=w_b(x,y,t)+w_s(x,y,t)$$

where u_0 and v_0 are the mid-plane displacements of the plate in the x and y directions, respectively; w_b and w_s are the bending and shear components of transverse displacement, respectively. It should be noted that unlike the FSDT, this theory does not require shear correction factors.

In this work, the present refined shear deformation plate theory is obtained by setting

$$f(z)=\frac{(h/\pi)\sinh\left(\frac{\pi}{h}z\right)-z}{\left[\cosh(\pi/2)-1\right]} \quad (5)$$

It can be seen that the displacement field in Eq. (4) introduces only four unknowns (u_0, v_0, w_b and w_s). The nonzero strains associated with the displacement field in Eq. (4) are

$$\begin{Bmatrix}\varepsilon_x\\ \varepsilon_y\\ \gamma_{xy}\end{Bmatrix}=\begin{Bmatrix}\varepsilon_x^0\\ \varepsilon_y^0\\ \gamma_{xy}^0\end{Bmatrix}+z\begin{Bmatrix}k_x^b\\ k_y^b\\ k_{xy}^b\end{Bmatrix}+f(z)\begin{Bmatrix}k_x^s\\ k_y^s\\ k_{xy}^s\end{Bmatrix}$$
$$\begin{Bmatrix}\gamma_{yz}\\ \gamma_{xz}\end{Bmatrix}=g(z)\begin{Bmatrix}\gamma_{yz}^s\\ \gamma_{xz}^s\end{Bmatrix}, \quad (6)$$

where

$$\left\{\begin{matrix}\varepsilon_x^0\\ \varepsilon_y^0\\ \gamma_{xy}^0\end{matrix}\right\}=\left\{\begin{matrix}\dfrac{\partial u_0}{\partial x}\\ \dfrac{\partial v_0}{\partial x}\\ \dfrac{\partial u_0}{\partial y}+\dfrac{\partial v_0}{\partial x}\end{matrix}\right\},\quad \left\{\begin{matrix}k_x^b\\ k_y^b\\ k_{xy}^b\end{matrix}\right\}=\left\{\begin{matrix}-\dfrac{\partial^2 w_b}{\partial x^2}\\ -\dfrac{\partial^2 w_b}{\partial y^2}\\ -2\dfrac{\partial^2 w_b}{\partial x\partial y}\end{matrix}\right\},$$
$$\left\{\begin{matrix}k_x^s\\ k_y^s\\ k_{xy}^s\end{matrix}\right\}=\left\{\begin{matrix}-\dfrac{\partial^2 w_s}{\partial x^2}\\ -\dfrac{\partial^2 w_s}{\partial y^2}\\ -2\dfrac{\partial^2 w_s}{\partial x\partial y}\end{matrix}\right\},\quad \left\{\begin{matrix}\gamma_{yz}^s\\ \gamma_{xz}^s\end{matrix}\right\}=\left\{\begin{matrix}\dfrac{\partial w_s}{\partial y}\\ \dfrac{\partial w_s}{\partial x}\end{matrix}\right\} \tag{7a}$$

and

$$g(z)=1-\frac{df(z)}{dz} \tag{7b}$$

2.3 Equations of motion

Hamilton's principle is herein utilized to determine the equations of motion

$$0=\int_0^t(\delta U-\delta T)\,dt \tag{8}$$

where δU is the variation of strain energy and δT is the variation of kinetic energy.

The variation of strain energy of the plate is given by

$$\begin{aligned}\delta U&=\int_V\left[\sigma_x\delta\varepsilon_x+\sigma_y\delta\varepsilon_y+\tau_{xy}\delta\gamma_{xy}+\tau_{yz}\delta\gamma_{yz}+\tau_{xz}\delta\gamma_{xz}\right]dV\\&=\int_A\left[N_x\delta\varepsilon_x^0+N_y\delta\varepsilon_y^0+N_{xy}\delta\gamma_{xy}^0+M_x^b\delta k_x^b+M_y^b\delta k_y^b+M_{xy}^b\delta k_{xy}^b\right.\\&\quad\left.+M_x^s\delta k_x^s+M_y^s\delta k_y^s+M_{xy}^s\delta k_{xy}^s+S_{yz}^s\delta\gamma_{yz}^s+S_{xz}^s\delta\gamma_{xz}^s\right]dA=0\end{aligned} \tag{9}$$

where A is the top surface and the stress resultants N, M, and S are defined by

$$\begin{aligned}&\left(N_i,M_i^b,M_i^s\right)=\int_{-h/2}^{h/2}(1,z,f)\sigma_i\,dz,\quad (i=x,y,xy)\\&\text{and}\quad\left(S_{xz}^s,S_{yz}^s\right)=\int_{-h/2}^{h/2}g\left(\tau_{xz},\tau_{yz}\right)dz\end{aligned} \tag{10}$$

The variation of kinetic energy of the plate can be expressed as

$$\begin{aligned}\delta T&=\int_{-\frac{h\Omega}{2}}^{\frac{h}{2}}\left[\ddot{u}\delta u+\ddot{v}\delta v+\ddot{w}\delta w\right]\rho(z)\,d\Omega\,dz\\&=\int_A\left\{I_0\left[\ddot{u}_0\delta u_0+\ddot{v}_0\delta v_0+\left(\ddot{w}_b+\ddot{w}_s\right)\left(\delta w_b+\delta w_s\right)\right]\right.\\&\quad-I_1\left(\ddot{u}_0\frac{\partial\delta w_b}{\partial x}+\frac{\partial\ddot{w}_b}{\partial x}\delta u_0+\ddot{v}_0\frac{\partial\delta w_b}{\partial y}+\frac{\partial\ddot{w}_b}{\partial y}\delta v_0\right)\\&\quad-I_2\left(\ddot{u}_0\frac{\partial\delta w_s}{\partial x}+\frac{\partial\ddot{w}_s}{\partial x}\delta u_0+\ddot{v}_0\frac{\partial\delta w_s}{\partial y}+\frac{\partial\ddot{w}_s}{\partial y}\delta v_0\right)\\&\quad+J_1\left(\frac{\partial\ddot{w}_b}{\partial x}\frac{\partial\delta w_b}{\partial x}+\frac{\partial\ddot{w}_b}{\partial y}\frac{\partial\delta w_b}{\partial y}\right)+K_2\left(\frac{\partial\ddot{w}_s}{\partial x}\frac{\partial\delta w_s}{\partial x}+\frac{\partial\ddot{w}_s}{\partial y}\frac{\partial\delta w_s}{\partial y}\right)\\&\quad\left.+J_2\left(\frac{\partial\ddot{w}_b}{\partial x}\frac{\partial\delta w_s}{\partial x}+\frac{\partial\ddot{w}_s}{\partial x}\frac{\partial\delta w_b}{\partial x}+\frac{\partial\ddot{w}_b}{\partial y}\frac{\partial\delta w_s}{\partial y}+\frac{\partial\ddot{w}_s}{\partial y}\frac{\partial\delta w_b}{\partial y}\right)\right\}d\Omega\end{aligned} \tag{11}$$

where dot-superscript convention indicates the differentiation with respect to the time variable t; $\rho(z)$ is the mass density given by Eq. (1); and $(I_i,\ J_i,\ K_i)$ are mass inertias expressed by

$$\left(I_0,I_1,I_2\right)=\int_{-h/2}^{h/2}\left(1,z,z^2\right)\rho(z)dz \tag{12a}$$

$$\left(J_1,J_2,K_2\right)=\int_{-h/2}^{h/2}\left(f,z\,f,f^2\right)\rho(z)dz \tag{12b}$$

By substituting Eqs. (9) and (11) into Eq. (8), the following can be derived

$$\begin{aligned}&\delta u_0:\ \frac{\partial N_x}{\partial x}+\frac{\partial N_{xy}}{\partial y}=I_0\ddot{u}_0-I_1\frac{\partial\ddot{w}_b}{\partial x}-J_1\frac{\partial\ddot{w}_s}{\partial x}\\&\delta v_0:\ \frac{\partial N_{xy}}{\partial x}+\frac{\partial N_y}{\partial y}=I_{01}\ddot{v}_0-I_1\frac{\partial\ddot{w}_b}{\partial y}-J_1\frac{\partial\ddot{w}_s}{\partial y}\\&\delta w_b:\ \frac{\partial^2M_x^b}{\partial x^2}+2\frac{\partial^2M_{xy}^b}{\partial x\partial y}+\frac{\partial^2M_y^b}{\partial y^2}=I_0\left(\ddot{w}_b+\ddot{w}_s\right)+I_1\left(\frac{\partial\ddot{u}_0}{\partial x}+\frac{\partial\ddot{v}_0}{\partial y}\right)-I_2\nabla^2\ddot{w}_b\\&\quad-J_2\nabla^2\ddot{w}_s\\&\delta w_s:\ \frac{\partial^2M_x^s}{\partial x^2}+2\frac{\partial^2M_{xy}^s}{\partial x\partial y}+\frac{\partial^2M_y^s}{\partial y^2}+\frac{\partial S_{xz}^s}{\partial x}+\frac{\partial S_{yz}^s}{\partial y}=I_0\left(\ddot{w}_b+\ddot{w}_s\right)+J_1\left(\frac{\partial\ddot{u}_0}{\partial x}+\frac{\partial\ddot{v}_0}{\partial y}\right)\\&\quad-J_2\nabla^2\ddot{w}_b-K_2\nabla^2\ddot{w}_s\end{aligned} \tag{13}$$

Substituting Eq. (6) into Eq. (2) and the subsequent results into Eq. (10), the stress resultants are obtained in terms of strains as following compact form

$$\left\{\begin{matrix}N\\ M^b\\ M^s\end{matrix}\right\}=\begin{bmatrix}A & B & B^s\\ B & D & D^s\\ B^s & D^s & H^s\end{bmatrix}\left\{\begin{matrix}\varepsilon\\ k^b\\ k^s\end{matrix}\right\},\quad S=A^s\gamma, \tag{14}$$

in which

$$\begin{aligned}&N=\left\{N_x,N_y,N_{xy}\right\}^t,\ M^b=\left\{M_x^b,M_y^b,M_{xy}^b\right\}^t,\\&M^s=\left\{M_x^s,M_y^s,M_{xy}^s\right\}^t,\end{aligned} \tag{15a}$$

$$\begin{aligned}&\varepsilon=\left\{\varepsilon_x^0,\varepsilon_y^0,\gamma_{xy}^0\right\}^t,\quad k^b=\left\{k_x^b,k_y^b,k_{xy}^b\right\}^t,\\&k^s=\left\{k_x^s,k_y^s,k_{xy}^s\right\}^t,\end{aligned} \tag{15b}$$

$$\begin{aligned}&A=\begin{bmatrix}A_{11}&A_{12}&0\\A_{12}&A_{22}&0\\0&0&A_{66}\end{bmatrix},\ B=\begin{bmatrix}B_{11}&B_{12}&0\\B_{12}&B_{22}&0\\0&0&B_{66}\end{bmatrix},\\&D=\begin{bmatrix}D_{11}&D_{12}&0\\D_{12}&D_{22}&0\\0&0&D_{66}\end{bmatrix},\end{aligned} \tag{15c}$$

$$\begin{aligned}&B^s=\begin{bmatrix}B_{11}^s&B_{12}^s&0\\B_{12}^s&B_{22}^s&0\\0&0&B_{66}^s\end{bmatrix},\ D^s=\begin{bmatrix}D_{11}^s&D_{12}^s&0\\D_{12}^s&D_{22}^s&0\\0&0&D_{66}^s\end{bmatrix},\\&H^s=\begin{bmatrix}H_{11}^s&H_{12}^s&0\\H_{12}^s&H_{22}^s&0\\0&0&H_{66}^s\end{bmatrix},\end{aligned} \tag{15d}$$

$$S=\left\{S_{xz}^{s},S_{yz}^{s}\right\}^{t},\quad \gamma=\left\{\gamma_{xz}^{s},\gamma_{yz}^{s}\right\}^{t},\quad A^{s}=\begin{bmatrix}A_{44}^{s} & 0\\ 0 & A_{55}^{s}\end{bmatrix}, \tag{15e}$$

and stiffness components are given as

$$\begin{Bmatrix}A_{11} & B_{11} & D_{11} & B_{11}^{s} & D_{11}^{s} & H_{11}^{s}\\ A_{12} & B_{12} & D_{12} & B_{12}^{s} & D_{12}^{s} & H_{12}^{s}\\ A_{66} & B_{66} & D_{66} & B_{66}^{s} & D_{66}^{s} & H_{66}^{s}\end{Bmatrix}=\int_{-h/2}^{h/2}Q_{11}\left(1,z,z^{2},f(z),zf(z),f^{2}(z)\right)\begin{Bmatrix}1\\ \nu\\ \frac{1-\nu}{2}\end{Bmatrix}dz \tag{16a}$$

$$\left(A_{22},B_{22},D_{22},B_{22}^{s},D_{22}^{s},H_{22}^{s}\right)=\left(A_{11},B_{11},D_{11},B_{11}^{s},D_{11}^{s},H_{11}^{s}\right) \tag{16b}$$

$$A_{44}^{s}=A_{55}^{s}=\int_{-h/2}^{h/2}Q_{44}\left[g(z)\right]^{2}dz, \tag{16c}$$

Introducing Eq. (14) into Eq. (13), the equations of motion can be expressed in terms of displacements (u_0, v_0, w_b and w_s) and the appropriate equations take the form

$$\begin{aligned}&A_{11}\frac{\partial^{2}u}{\partial x^{2}}+A_{66}\frac{\partial^{2}u}{\partial y^{2}}+\left(A_{12}+A_{66}\right)\frac{\partial^{2}v}{\partial x\partial y}-B_{11}\frac{\partial^{3}w_{b}}{\partial x^{3}}-\left(B_{12}+2B_{66}\right)\frac{\partial^{3}w_{b}}{\partial x\partial y^{2}}\\&-B_{11}^{s}\frac{\partial^{3}w_{s}}{\partial x^{3}}-\left(B_{12}^{s}+2B_{66}^{s}\right)\frac{\partial^{3}w_{s}}{\partial x\partial y^{2}}=I_{0}\ddot{u}_{0}-I_{1}\frac{\partial\ddot{w}_{b}}{\partial x}-J_{1}\frac{\partial\ddot{w}_{s}}{\partial x},\end{aligned} \tag{17a}$$

$$\begin{aligned}&\left(A_{12}+A_{66}\right)\frac{\partial^{2}u}{\partial x\partial y}+A_{66}\frac{\partial^{2}v}{\partial x^{2}}+A_{22}\frac{\partial^{2}v}{\partial y^{2}}-\left(B_{12}+2B_{66}\right)\frac{\partial^{3}w_{b}}{\partial x^{2}\partial y}-B_{22}\frac{\partial^{3}w_{b}}{\partial y^{3}}\\&-B_{22}^{s}\frac{\partial^{3}w_{s}}{\partial y^{3}}-\left(B_{12}^{s}+2B_{66}^{s}\right)\frac{\partial^{3}w_{s}}{\partial x^{2}\partial y}=I_{0}\ddot{v}_{0}-I_{1}\frac{\partial\ddot{w}_{b}}{\partial y}-J_{1}\frac{\partial\ddot{w}_{s}}{\partial y}\end{aligned} \tag{17b}$$

$$\begin{aligned}&B_{11}\frac{\partial^{3}u}{\partial x^{3}}+\left(B_{12}+2B_{66}\right)\frac{\partial^{3}u}{\partial x\partial y^{2}}+\left(B_{12}+2B_{66}\right)\frac{\partial^{3}v}{\partial x^{2}\partial y}+B_{22}\frac{\partial^{3}v}{\partial y^{3}}-D_{11}\frac{\partial^{4}w_{b}}{\partial x^{4}}\\&-2\left(D_{12}+2D_{66}\right)\frac{\partial^{4}w_{b}}{\partial x^{2}\partial y^{2}}-D_{22}\frac{\partial^{4}w_{b}}{\partial y^{4}}-D_{11}^{s}\frac{\partial^{4}w_{s}}{\partial x^{4}}-2\left(D_{12}^{s}+2D_{66}^{s}\right)\frac{\partial^{4}w_{s}}{\partial x^{2}\partial y^{2}}\\&-D_{22}^{s}\frac{\partial^{4}w_{s}}{\partial y^{4}}=I_{0}\left(\ddot{w}_{b}+\ddot{w}_{s}\right)+I_{1}\left(\frac{\partial\ddot{u}_{0}}{\partial x}+\frac{\partial\ddot{v}_{0}}{\partial y}\right)-I_{2}\nabla^{2}\ddot{w}_{b}-J_{2}\nabla^{2}\ddot{w}_{s},\end{aligned} \tag{17c}$$

$$\begin{aligned}&B_{11}^{s}\frac{\partial^{3}u}{\partial x^{3}}+\left(B_{12}^{s}+2B_{66}^{s}\right)\frac{\partial^{3}u}{\partial x\partial y^{2}}+\left(B_{12}^{s}+2B_{66}^{s}\right)\frac{\partial^{3}v}{\partial x^{2}\partial y}+B_{22}^{s}\frac{\partial^{3}v}{\partial y^{3}}-D_{11}^{s}\frac{\partial^{4}w_{b}}{\partial x^{4}}\\&-2\left(D_{12}^{s}+2D_{66}^{s}\right)\frac{\partial^{4}w_{b}}{\partial x^{2}\partial y^{2}}-D_{22}^{s}\frac{\partial^{4}w_{b}}{\partial y^{4}}-H_{11}^{s}\frac{\partial^{4}w_{s}}{\partial x^{4}}-2\left(H_{12}^{s}+2H_{66}^{s}\right)\frac{\partial^{4}w_{s}}{\partial x^{2}\partial y^{2}}-H_{22}^{s}\frac{\partial^{4}w_{s}}{\partial y^{4}}\\&+A_{55}^{s}\frac{\partial^{2}w_{s}}{\partial x^{2}}+A_{44}^{s}\frac{\partial^{2}w_{s}}{\partial y^{2}}=I_{0}\left(\ddot{w}_{b}+\ddot{w}_{s}\right)+J_{1}\left(\frac{\partial\ddot{u}_{0}}{\partial x}+\frac{\partial\ddot{v}_{0}}{\partial y}\right)-J_{2}\nabla^{2}\ddot{w}_{b}-K_{2}\nabla^{2}\ddot{w}_{s}\end{aligned} \tag{17d}$$

Clearly, when the effect of transverse shear deformation is neglected w_s, Eq. (17) yields the equations of motion of FG plate based on the CPT.

2.4 Exact solutions for FGM plates

The determination of frequency is of fundamental importance in the design of many structural components. An exact closed-form solution to Eq. (17) can be constructed when the plate is of a rectangular geometry with the following edge conditions, displacements.

2.4.1 Boundary conditions

The present vibration problem accounts for various cases of boundary conditions at the opposite edges x=0 and a, i.e., these plate edges are simply-supported (S), clamped (C), free (F) or a combination of these boundary conditions. While the edges y=0 and b are invariably simply-supported (i.e., $u=w_b=w_s=N_y=M_y^b=M_y^s=0$). The boundary conditions on the edges perpendicular to x-axis take the form

Simply supported (S)

$$v=w_b=w_s=N_x=M_x^b=M_x^s=0 \tag{18a}$$

Clamped (C)

$$u=v=w_b=w_s=N_x=\frac{\partial w_b}{\partial x}=\frac{\partial w_s}{\partial x}=0 \tag{18b}$$

and free (F)

$$N_x=N_{xy}=M_x^b=M_x^s=0 \tag{18c}$$

2.4.2 Displacements

Rectangular plates are generally classified in accordance with the type support used in the absence of the body forces and lateral loads. The solution of the system of partial differential Eqs. (18) under conditions (18) may be expressed as

$$\begin{Bmatrix}u_0\\ v_0\\ w_b\\ w_s\end{Bmatrix}=\begin{Bmatrix}U_{mn}F^{'}(x)\sin(\mu y)e^{i\omega t}\\ V_{mn}F^{'}(x)\cos(\mu y)e^{i\omega t}\\ W_{bmn}F(x)\sin(\mu y)e^{i\omega t}\\ W_{smn}F(x)\sin(\mu y)e^{i\omega t}\end{Bmatrix} \tag{19}$$

where U_{mn}; V_{mn}; W_{bmn}; and W_{smn} are arbitrary parameters to be determined subjected to the conditions that the solution in Eqs. (19) satisfies the differential Eqs. (17), $\mu=n\pi/b$ and m and n are mode numbers. $(\,)'$ denotes the partial differentiation with respect to x. The function $F(x)$ is a continuous arbitrary function, which satisfy at least the geometric boundary conditions given in (18), and represents approximate shapes of the deflected surface of the plate.

This function, for the different cases of boundary conditions, takes the following forms (Reddy 2004)

$$\begin{aligned}&\text{SS}:\ F(x)=\sin(\lambda_m x),\quad \lambda_m=m\pi/a.\\&\text{CC}:\ F(x)=\sin(\lambda_m x)-\sinh(\lambda_m x)-\zeta_m\left[\cos(\lambda_m x)-\cosh(\lambda_m x)\right],\\&\zeta_m=\left[\sin(\lambda_m a)-\sinh(\lambda_m a)\right]/\left[\cos(\lambda_m a)-\cosh(\lambda_m a)\right],\\&\lambda_m=(m+0.5)\pi/a.\\&\text{CS}:\ F(x)=\sin(\lambda_m x)-\sinh(\lambda_m x)-\zeta_m\left[\cos(\lambda_m x)-\cosh(\lambda_m x)\right],\\&\zeta_m=\left[\sin(\lambda_m a)+\sinh(\lambda_m a)\right]/\left[\cos(\lambda_m a)+\cosh(\lambda_m a)\right],\\&\lambda_m=(m+0.25)\pi/a.\\&\text{CF}:\ F(x)=\sin(\lambda_m x)-\sinh(\lambda_m x)-\zeta_m\left[\cos(\lambda_m x)-\cosh(\lambda_m x)\right],\\&\zeta_m=\left[\sin(\lambda_m a)-\sinh(\lambda_m a)\right]/\left[\cos(\lambda_m a)-\cosh(\lambda_m a)\right],\\&\lambda_1=1.875/a,\quad \lambda_2=4.694/a,\quad \lambda_3=7.855/a,\\&\lambda_4=10.966/a,\\&\lambda_m=(m-0.25)\pi/a\ \text{ for }\ m\geq 5.\end{aligned} \tag{20}$$

Substituting Eqs. (19) into Eq. (17), one obtains

$$\begin{Bmatrix} u_0 \\ v_0 \\ w_b \\ w_s \end{Bmatrix} = \begin{Bmatrix} U_{mn}F^{'}(x)\sin(\mu y)e^{i\omega t} \\ V_{mn}F^{'}(x)\cos(\mu y)e^{i\omega t} \\ W_{bmn}F(x)\sin(\mu y)e^{i\omega t} \\ W_{smn}F(x)\sin(\mu y)e^{i\omega t} \end{Bmatrix} \tag{21}$$

where

$$\begin{aligned}
&S_{11} = \left(A_{11}\beta_5 - A_{66}\mu^2\beta_4\right), \quad S_{12} = -\mu\left(A_{12} + A_{66}\right)\beta_4, \\
&S_{13} = -B_{11}\beta_5 + \mu^2\left(B_{12} + 2B_{66}\right)\beta_4, \\
&S_{14} = -B^s_{11}\beta_5 + \left(B^s_{12} + 2B^s_{66}\right)\beta_4, \quad S_{21} = \left(A_{12} + A_{66}\right)\mu\beta_2, \\
&S_{22} = \left(-A_{22}\mu^2\beta_1 + A_{66}\beta_2\right), \\
&S_{23} = B_{22}\mu^3\beta_1 - \left(B_{12} + 2B_{66}\right)\mu\beta_2, \\
&S_{24} = \left(B^s_{12} + 2B^s_{66}\right)\mu\beta_2 + B^s_{22}\mu^3\beta_1, \\
&S_{31} = B_{11}\beta_3 - \left(B_{12} + 2B_{66}\right)\mu^2\beta_2, \\
&S_{32} = -\left(B_{12} + 2B_{66}\right)\mu\beta_2 + B_{22}\mu^3\beta_1, \\
&S_{33} = -D_{11}\beta_3 + 2\left(D_{12} + 2D_{66}\right)\mu^2\beta_2 - .D_{22}\mu^4\beta_1, \\
&S_{34} = -D^s_{11}\beta_3 + 2\left(D^s_{11} + 2D^s_{66}\right)\mu^2\beta_2 - .D^s_{22}\mu^4\beta_1, \\
&S_{41} = B^s_{11}\beta_3 - \left(B^s_{11} + 2B^s_{66}\right)\mu^2\beta_2, \\
&S_{42} = -.\left(B^s_{12} + 2B^s_{66}\right)\mu\beta_2 + B^s_{22}\mu^3\beta_1, \\
&S_{43} = -D^s_{11}\beta_3 + 2\left(D^s_{12} + 2D^s_{66}\right)\mu^2\beta_2 - .D^s_{22}\mu^4\beta_1, \\
&S_{44} = -H^s_{11} + 2\left(H^s_{12} + 2H^s_{66}\right)\mu^2\beta_2 - .H^s_{22}\mu^4\beta_1 + A^s_{55}\beta_2 - A^s_{44}\mu^2\beta_1, \\
&m_{11} = -I_1\beta_4, \ m_{12} = 0, \ m_{13} = I_2\beta_4, \ m_{14} = I_4\beta_4, \\
&m_{21} = 0, \ m_{22} = -I_1\beta_1, \ m_{23} = I_2\mu\beta_1, \ m_{24} = I_4\mu\beta_1, \\
&m_{31} = -I_2\beta_2, \\
&m_{32} = I_2\mu\beta_1, \ m_{33} = -\left(I_1\beta_1 - I_3\left(\beta_2 - \mu^2\beta_1\right)\right), \\
&m_{34} = -\left(I_1\beta_1 - I_5\left(\beta_2 - \mu^2\beta_1\right)\right), \ m_{41} = -I_1\beta_2, \\
&m_{42} = I_4\mu\beta_1, \ m_{43} = -\left(I_1\beta_1 - I_5\left(\beta_2 - \mu^2\beta_1\right)\right), \\
&m_{44} = -\left(I_1\beta_1 - I_6\left(\beta_2 - \mu^2\beta_1\right)\right),
\end{aligned} \tag{22}$$

in which

$$\begin{aligned}
&\beta_1 = \int_0^a [F(x)]^2\,dx, \quad \beta_2 = \int_0^a F(x)F^{''}(x)dx, \\
&\beta_3 = \int_0^a F(x)F^{''''}(x)dx, \quad \beta_4 = \int_0^a [F^{'}(x)]^2\,dx, \\
&\beta_5 = \int_0^a F^{'}(x)F^{'''}(x)dx,
\end{aligned} \tag{23}$$

3. Results and discussion

Two types of FG plates of Al/Al_2O_3 and Al/ZrO_2 are used in this study which their material properties are listed in Table 1. For convenience, a two-letter notation is used to describe the boundary conditions of the remaining edges. For instance, FC indicates that one edge is free (F) and the other is clamped (C). For verification purpose, the obtained solutions are compared with those available in open literature and those computed independently for the first time based on CPT, FSDT, and HSDT of Reddy. For all calculations, the shear correction factor and Poisson's ratio are taken as 5/6 and 0.3, respectively. For convenience, following natural frequency parameter is used

Table 1 Material properties of FG plate used in this study

Properties	Metal	Ceramic	
	Aluminum (Al)	Alumina (Al_2O_3)	Zirconia (ZrO_2)
$E(GPa)$	70	380	200
$\rho(kg/m^3)$	2702	3800	5700

$$\begin{aligned}
&\overline{\beta} = \omega h\sqrt{\rho_m / E_m}; \\
&\hat{\beta} = \omega h\sqrt{\rho_c / E_c}; \\
&\overline{\omega} = \omega a^2\left(\sqrt{\rho_c / E_c}\right)/ h;
\end{aligned} \tag{24}$$

3.1 Comparison Studies

The first example is carried out for simply supported Al/ZrO_2 square plates with different values of thickness ratio a/h and power law index *p*. Table 2 shows the comparison of fundamental frequency parameters $\overline{\beta}$ obtained in this study with those given by Vel and Batra (2004) based on 3-D theory, Matsunaga (2008) based on 2-D theory, Pradyumna and Bandyopadhyay (2008) based on HSDT, Hosseini-Hashemi *et al.* (2011b) based on Reddy's theory, Hosseini-Hashemi *et al.* (2011a) based on FSDT and Tai *et al.* (2014) based on a refined plate theory. It can be seen that for the plate with p = 0, i.e., fully ceramic isotropic plate, the results of present theory are well agreement with those of 3-D, HSDT, and FSDT solutions. However, for FG plate with non-zero values of *p*, the results of present theory and other shear deformation theories are higher than those obtained by 3-D exact solutions of Vel and Batra (2004). The reason for this feature may be due to the way to estimate the material properties of FG plates. In Vel and Batra (2004), the material properties at a point were estimated from the local volume fractions using Mori-Tanaka scheme (Mori and Tanaka 1973), whereas in present and other studies, the material properties are assumed to vary through the thickness of the plate with a power law distribution of the volume fractions of the two materials. The CPT overestimates the frequency of FG plates compared to the shear deformation theories and 3-D solutions. The difference between CPT and shear deformation theories and 3-D solutions is more considerable for thick plates.

For example, the difference between the CPT and the present theory, for fully ceramic plate, increases from 2.59% to 19.75% when the *a*/*h* ratio is decreased from 10 to $\sqrt{10}$. It is observed that there is an excellent agreement between the results obtained by present theory and Reddy's theory (Hosseini-Hashemi *et al.* 2011b), and the results computed independently in this study based on FSDT and HSDT coincide with those reported in open literature. It should be noted that the present theory involves four unknowns as against five unknowns in the case of FSDT and HSDT of Reddy.

The next comparison is carried out for SS Al/Al_2O_3 square plates. Frequency parameters $\hat{\beta}$ are shown in Table

Table 2 Comparison of fundamental frequency parameter $\overline{\beta}$ of SS Al/ZrO_2 square plate

Theory	p=0					a/h=5		
	$a/h=\sqrt{10}$	a/h=10	a/h=5	a/h=10	a/h=20	p=2	p=3	p=5
3-D (Vel and Batra 2004)	0.4658	0.0578	0.2192	0.0596	0.0153	0.2197	0.2211	0.2225
HSDT (Matsunaga 2008)	0.4658	0.0578	0.2285	0.0619	0.0158	0.2264	0.2270	0.2281
HSDT (Pradyumna and Bandyopadhyay 2008)	0.4658	0.0578	0.2257	0.0613	0.0157	0.2237	0.2243	0.2253
HSDT (Hosseini-Hashemi *et al.* 2011b)	0.4623	0.0577	0.2276	0.0619	0.0158	0.2256	0.2263	0.2272
FSDT (Hosseini-Hashemi *et al.* 2011a)	0.4618	0.0577	0.2276	0.0619	0.0158	0.2264	0.2276	0.2291
HSDT[a]	0.4623	0.0577	0.2277	0.0619	0.0158	0.2257	0.2263	0.2272
FSDT[a]	0.4618	0.0577	0.2276	0.0619	0.0158	0.2264	0.2276	0.2291
CPT[a]	0.5535	0.0592	0.2479	0.0634	0.0159	0.2473	0.2497	0.2526
Tai *et al.* 2014	0.4623	0.0577	0.2277	0.0619	0.0158	0.2257	0.2263	0.2272
Present	0.4622	0.0577	0.2277	0.0619	0.0158	0.2257	0.2263	0.2272

[a] Results from Tai and Ho (2014)

3. It can be seen that the results obtained by present theory are good agreement with those reported by Matsunaga (2008) based on 2-D theory, Hosseini-Hashemi *et al*. (2011b) based on HSDT, and Hosseini-Hashemi *et al*. (2011a) based on FSDT. Also, the results computed independently in this study based on FSDT, HSDT and the refined plate theory of Tai *et al*. (2014) coincide with those reported in the literature. The results also indicate that the CPT overestimates the natural frequency of FG plates, and the difference between the CPT and present theory is considerable for thick plate at higher modes of vibration.

The variations of fundamental frequency parameter $\overline{\omega}$ with respect to power law index p and thickness ratio a/h are shown in Fig. 2 and 3, respectively. Compared to the refined plate theory of Tai *et al*. (2014), it can be observed that the frequency obtained using the present theory is in good agreement with those given by the refined plate theory of Tai *et al*. (2014) for all values of power law index p and thickness ratio a/h and various boundary conditions.

3.2 Parameter Studies

After verifying the accuracy of the present solution, parameter studies are carried out to investigate the effects of variations of power law index, thickness ratio, and aspect ratio on natural frequency of Al/Al_2O_3 plates. Based on the present solutions, the variations of fundamental frequency parameters $\overline{\omega}$ of FG plates with respect to power law index p, thickness ratio a/h and aspect ratio b/a are illustrated in Figs. 4-6, respectively. Furthermore, comprehensive results are tabulated in Tables 5-8 for Al/Al_2O_3 plates with different boundary conditions.

In each table, the aspect ratio b/a are taken to be 0.5, 1 and 2, while three different values of thickness ratios a/h are examined. In addition, six arbitrary values of the power law index p are considered. The following points can be noticeable from Figs. 4-6 and Tables 5-8:

-Regardless of boundary condition, thickness ratio, and aspect ratio, the frequency parameter drops as the power law index increases. A prominent drop in frequency occurs when the power law index varies between 0 and 2 (see Fig. 4). This is due to the fact that increasing the power law index increases the volume fraction of metal.

Table 3 Comparison of natural frequency parameter $\hat{\beta}$ of SS Al/Al_2O_3 square plate

a/h	Mode	Method	Power law index, p				
			0	0.5	1	4	10
5	1	HSDT (Matsunaga, 2008)	0.2121	0.1819	0.1640	0.1383	0.1306
		HSDT (Hosseini-Hashemi *et al.* 2011b)	0.2113	0.1807	0.1631	0.1378	0.1301
		FSDT (Hosseini-Hashemi *et al.* 2011a)	0.2112	0.1805	0.1631	0.1397	0.1324
		HSDT[a]	0.2113	0.1807	0.1631	0.1378	0.1301
		FSDT[a]	0.2112	0.1805	0.1631	0.1397	0.1324
		CPT[a]	0.2314	0.1959	0.1762	0.1524	0.1467
		Tai *et al.* (2014)	0.2113	0.1807	0.1631	0.1378	0.1301
		Present	0.2113	0.1807	0.1631	0.1379	0.1301
	2	HSDT (Matsunaga 2008)	0.4658	0.4040	0.3644	0.3000	0.2790
		HSDT (Hosseini-Hashemi *et al.* 2011b)	0.4623	0.3989	0.3607	0.2980	0.2771
		FSDT (Hosseini-Hashemi *et al.* 2011a)	0.4618	0.3978	0.3604	0.3049	0.2856
		HSDT[a]	0.4623	0.3989	0.3607	0.2980	0.2771
		FSDT[a]	0.4618	0.3978	0.3604	0.3049	0.2856
		CPTa	0.5535	0.4681	0.4198	0.3603	0.3481
		Tai et al. 2014	0.4623	0.3989	0.3607	0.2980	0.2771
		Present	0.4622	0.3989	0.3607	0.2982	0.2772
10	1	HSDT (Matsunaga 2008)	0.0577	0.0492	0.0443	0.0381	0.0364
		HSDT (Hosseini-Hashemi *et al.* 2011b)	0.0577	0.0490	0.0442	0.0381	0.0364
		FSDT (Hosseini-Hashemi *et al.* 2011a)	0.0577	0.0490	0.0442	0.0382	0.0366
		HSDT[a]	0.0577	0.0490	0.0442	0.0381	0.0364
		FSDT[a]	0.0577	0.0490	0.0442	0.0382	0.0366
		CPT[a]	0.0592	0.0502	0.0452	0.0392	0.0377
		Tai et al. 2014	0.0577	0.0490	0.0442	0.0381	0.0364
		Present	0.0577	0.0490	0.0442	0.0381	0.0364
	2	HSDT (Matsunaga, 2008)	0.1381	0.1180	0.1063	0.0904	0.0859
		HSDT (Hosseini-Hashemi *et al.* 2011b)	0.1377	0.1174	0.1059	0.0903	0.0856
		FSDT (Hosseini-Hashemi *et al.* 2011a)	0.1376	0.1173	0.1059	0.0911	0.0867
		HSDT[a]	0.1376	0.1174	0.1059	0.0902	0.0856
		FSDT[a]	0.1376	0.1173	0.1059	0.0911	0.0867
		CPT[a]	0.1464	0.1239	0.1115	0.0966	0.0930
		Tai *et al.* (2014)	0.1376	0.1174	0.1059	0.0902	0.0856
		Present	0.1376	0.1174	0.1059	0.0902	0.0856
20	1	HSDT (Hosseini-Hashemi *et al.* 2011b)	0.0148	0.0125	0.0113	0.0098	0.0094
		FSDT (Hosseini-Hashemi *et al.* 2011a)	0.0148	0.0125	0.0113	0.0098	0.0094
		HSDT[a]	0.0148	0.0125	0.0113	0.0098	0.0094
		FSDT[a]	0.0148	0.0125	0.0113	0.0098	0.0094
		CPT[a]	0.0149	0.0126	0.0114	0.0099	0.0095
		Tai *et al.* 2014	0.0148	0.0125	0.0113	0.0098	0.0094
		Present	0.0148	0.0125	0.0113	0.0098	0.0094

[a] Results from Ref. (Tai and Ho 2014).

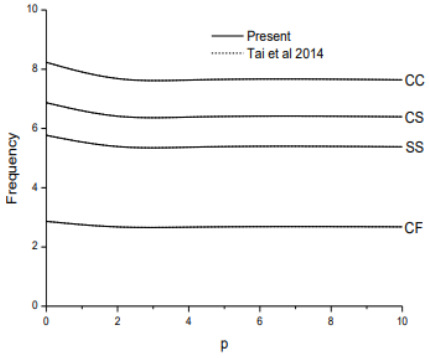

Fig. 2 Comparison of the variation of fundamental frequency parameter $\bar{\omega}$ of Al/ZrO2 Square Plate versus power law index p when a/h=10

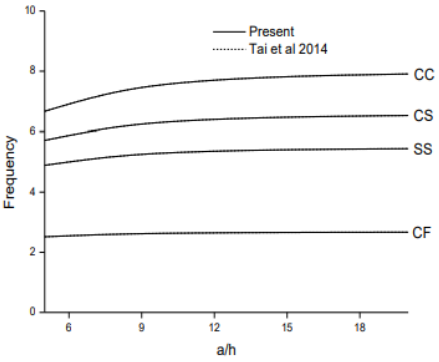

Fig. 3 Comparison of the variation of fundamental frequency parameter $\bar{\omega}$ of Al/ZrO_2 square plate versus thickness ratio a/h when p=1

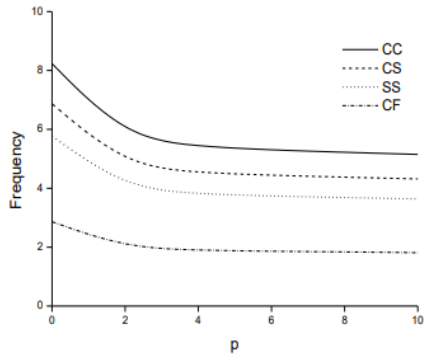

Fig. 4 Effect of power law index p on fundamental frequency parameter $\bar{\omega}$ of Al/Al_2O_3 Square Plate when a/h=10

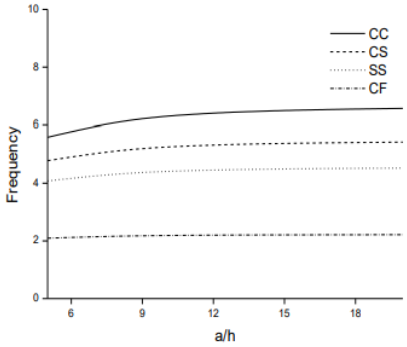

Fig. 5 Effect of thickness ratio a/h on fundamental frequency parameter $\bar{\omega}$ of Al/Al_2O_3 square plate when p=1

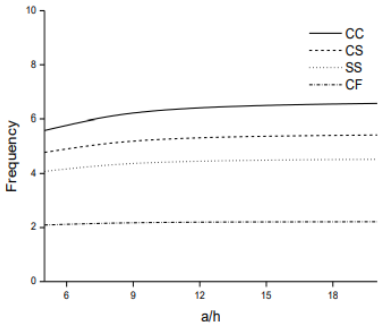

Fig. 6 Effect of aspect ratio b/a on fundamental frequency parameter $\bar{\omega}$ of Al/Al2O3 rectangular plate when a/h=10 and p=1

Table 5 Fundamental frequency parameter $\bar{\omega}$ of CC Al/Al2O3 plate

a/b	*a/h*	Power law index, *p*				
		0	0.5	1	5	10
0.5	5	5.9081	5.0932	4.6108	3.7608	3.5693
	10	6.7644	5.7627	5.2008	4.4003	4.2315
	20	7.0523	5.9825	5.3936	4.6267	4.4719
1.0	5	7.1719	6.1781	5.5894	4.5637	4.3360
	10	8.2312	7.0111	6.3261	5.3526	5.1489
	20	8.5931	7.2893	6.5714	5.6368	5.4486
2.0	5	12.4913	10.8040	9.7779	7.8702	7.4494
	10	15.1495	12.9337	11.6720	9.7914	9.3965
	20	16.2033	13.7554	12.4013	10.6064	10.2437

Table 6 Fundamental frequency parameter $\bar{\omega}$ of CS Al/Al_2O_3 Plate

a/b	*a/h*	Power law index, *p*				
		0	0.5	1	5	10
0.5	5	4.6336	3.9686	3.5850	2.9791	2.8482
	10	5.0677	4.3068	3.8839	3.3107	3.1933
	20	5.2007	4.4087	3.9739	3.4162	3.3048
1.0	5	6.1660	5.2890	4.7781	3.9482	3.7693
	10	6.8697	5.8419	5.2685	4.4799	4.3181
	20	7.0959	6.0164	5.4231	4.6587	4.5058
2.0	5	12.0278	10.3884	9.3966	7.5917	7.1971
	10	14.4399	12.3198	11.1157	9.3429	8.9733
	20	15.3756	13.0500	11.7646	10.0684	9.7267

Table 7 Fundamental frequency parameter $\bar{\omega}$ of SS Al/Al_2O_3 plate

a/b	*a/h*	Power law index, *p*				
		0	0.5	1	5	10
0.5	5	3.4413	2.9347	2.6476	2.2285	2.1414
	10	3.6518	3.0990	2.7937	2.3921	2.3112
	20	3.7123	3.1458	2.8352	2.4403	2.3619
1.0	5	5.2815	4.5181	4.0782	3.3967	3.2529
	10	5.7695	4.9015	4.4193	3.7693	3.6375
	20	5.9199	5.0179	4.5228	3.8886	3.7624

Table 7 Continued

a/b	a/h	Power law index, p				
		0	0.5	1	5	10
2.0	5	11.5562	9.9714	9.0165	7.3040	6.9318
	10	13.7655	11.7390	10.5904	8.9141	8.5659
	20	14.6073	12.3961	11.1748	9.5682	9.2451

Table 8 Fundamental frequency parameter $\overline{\omega}$ of CF Al/Al_2O_3 plate

a/b	a/h	Power law index, p				
		0	0.5	1	5	10
0.5	5	1.0849	0.9239	0.8339	0.7064	0.6795
	10	1.1259	0.9551	0.8610	0.7389	0.7143
	20	1.1370	0.9634	0.8683	0.7478	0.7239
1.0	5	2.7254	2.3219	2.0946	1.7689	1.7015
	10	2.8635	2.4293	2.1899	1.8772	1.8144
	20	2.9022	2.4591	2.2163	1.9083	1.8471
2.0	5	9.4721	8.1526	7.3677	6.0157	5.7241
	10	10.9883	9.3589	8.4416	7.1359	6.8667
	20	11.5290	9.7799	8.8158	7.5591	7.3073

-Regardless of boundary condition, aspect ratio, and power law index, the frequency parameter increases with the increase of thickness ratio *a*/*h*. The increase of frequency becomes significant for thick plate with $a/h\pi5$ (see Fig. 5). Such behavior is due to the influence of rotary inertia and shear deformations.

-Regardless of boundary condition, thickness ratio, and power law index, the frequency parameter decreases by increasing the aspect ratio b/a (see Fig. 6).

-Regardless of aspect ratio, thickness ratio, and power law index, the frequency parameter increases when higher restraining boundary condition is used at the other two edges of plates. In other words, the lowest and highest values of frequency correspond to the CF and CC plates, respectively (see Figs. 4-6). Such behavior is due to the fact that higher constraints at the edges increase the flexural rigidity of the plate, leading to a higher frequency response.

4. Conclusions

An efficient and simple refined shear deformation theory is successfully developed for FG plates with two opposite edges simply supported and the other two edges having arbitrary boundary conditions. The RPT accounts for quadratic variation of the transverse shear strains across the thickness, and satisfies the zero traction boundary conditions on the top and bottom surfaces of the plate without using shear correction factors. The effects of many parameters on the free vibration in FGM plates under various boundary conditions are all investigated. The results of present theory with four independent variables are comparable with those generated by other shear deformation plate theories containing more number of independent variables.

References

Al-Basyouni, K.S., Tounsi, A. and Mahmoud, S.R. (2015), "Size dependent bending and vibration analysis of functionally graded micro beams based on modified couple stress theory and neutral surface position", *Compos. Struct.*, **125**, 621-630.

Arani, A.G., Haghparast, E. and Zarei, H.B. (2017), "Vibration analysis of functionally graded nanocomposite plate moving in two directions", *Compos. Struct.*, **23**(5), 529-541.

Belabed, Z., Houari, M.S.A., Tounsi, A., Mahmoud, S.R. and Bég, O.A (2014), "An efficient and simple higher order shear and normal deformation theory for functionally graded material (FGM) plates", *Compos. Part B*, **60**, 274-283.

Benahmed, A., Houari, M.S.A., Benyoucef, S., Belakhdar, K. and Tounsi, A. (2017), "A novel quasi-3D hyperbolic shear deformation theory for functionally graded thick rectangular plates on elastic foundation", *Geomech. Eng.*, **12**(1), 9-34.

Benbakhti, A., Bouiadjra, M.B., Retiel, N. and Tounsi, A. (2016), "A new five unknown quasi-3D type HSDT for thermomechanical bending analysis of FGM sandwich plates", *Steel Compos. Struct.*, **22**(5), 975-999.

Benferhat, R., Hassaine, D., Hadji, L. and Said, M. (2016), "Static analysis of the FGM plate with porosities", *Steel Compos. Struct.*, **21**(1), 123-136.

Deng, H.Q., Li, T.J., Xue, B.J. and Wang, Z.W. (2015), "Analysis of thermally induced vibration of cable-beam structures", *Struct. Eng. Mech.*, **53**(3), 443-453.

Farahani, H. and Barati, F. (2015), "Vibration of sumberged functionally graded cylindrical shell based on first order shear deformation theory using wave propagation method", *Struct. Eng. Mech.*, **53**(3), 575-587.

Gao, Y., Yu, L.Y., Yang, L.Z. and Zhang, L.L. (2015), "The refined theory of 2D quasicrystal deep beams based on elasticity of quasicrystals", *Struct. Eng. Mech.*, **53**(3), 411-427.

Hadji, L., Zouatnia, N. and Kassoul, A. (2017), "Wave propagation in functionally graded beams using various higher-order shear deformation beams theories", *Struct. Eng. Mech.*, **62**(2), 143-149.

Hamidi, A., Houari, M.S.A., Mahmoud, S.R. and Tounsi, A. (2015), "A sinusoidal plate theory with 5-unknowns and stretching effect for thermomechanical bending of functionally graded sandwich plates", *Steel Compos. Struct.*, **18**(1), 235-253.

Hebali, H., Tounsi, A., Houari, M.S.A., Bessaim, A. and Bedia, E.A.A (2014), "A new quasi-3D hyperbolic shear deformation theory for the static and free vibration analysis of functionally graded plates", *J. Eng. Mech.*, **140**(2), 374-383.

Hosseini-Hashemi, S., Fadaee, M. and Atashipour, S.R. (2011b), "Study on the free vibration of thick functionally graded rectangular plates according to a new exact closed-form procedure", *Compos. Struct.*, **93**(2), 722-735.

Hosseini-Hashemi, S., Fadaee, M. and Atashipour, S.R. (2011a), "A new exact analytical approach for free vibration of Reissner-Mindlin functionally graded rectangular plates", *J. Mech. Sci.*, **53**(1), 11-22.

Matsunaga, H. (2008), "Free vibration and stability of functionally graded plates according to a 2-D higher-order deformation theory", *Compos. Struct.*, **82**(4), 499-512.

Merazi, M., Hadji, L., Daouadji, T.H., Tounsi, A. and Adda, B. (2015), "A new hyperbolic shear deformation plate theory for static analysis of FGM plate based on neutral surface position", *Geomech. Eng.*, **8**(3), 305-321.

Meziane, M.A.A., Abdelaziz, H.H. and Tounsi, A. (2014), "An efficient and simple refined theory for buckling and free

vibration of exponentially graded sandwich plates under various boundary conditions", *J. Sandw. Struct. Mater.*, **16**(3), 293-318.
Pradyumna, S. and Bandyopadhyay, J.N. (2008), "Free vibration analysis of functionally graded curved panels using a higher-order finite element formulation", *J. Sound Vib.*, **318**(1-2), 176-192.
Reddy, J.N. (2004), *Mechanics of Laminated Composite Plates and Shells: Theory and Analysis*, CRC Press, Boca Raton, Florida, U.S.A.
Sobhy, M. (2013), "Buckling and free vibration of exponentially graded sandwich plates resting on elastic foundations under various boundary conditions", *Compos. Struct.*, **99**, 76-87.
Tahouneh, V. (2014), "Free vibration analysis of bidirectional functionally graded annular plates resting on elastic foundations using differential quadrature method", *Struct. Eng. Mech.*, **52**(4), 663-686.
Tai, H.T. and Choi, D.H. (2014), "Levy solution for free vibration analysis of functionally graded plates based on a refined plate theory, *KSCE J. Civ. Eng.*, **18**(6),1813-1824.
Tai, H.T. and Kim, S.E. (2011), "Levy-type solution for buckling analysis of orthotropic plates based on two variable refined plate theory", *Compos. Struct.*, **93**(7), 1738-1746.
Tai, H.T. and Kim, S.E. (2012), "Levy-type solution for free vibration analysis of orthotropic plates based on two variable refined plate theory", *Appl. Math. Modell.*, **36**(8), 3870-3882.
Vel, S.S. and Batra, R.C. (2004), "Three-dimensional exact solution for the vibration of functionally graded rectangular plates", *J. Sound Vib.*, **272**(3-5), 703-730.

CC